Three-Dimensional Structure of Normal Shock Wave/Turbulent Boundary Layer Interaction in a Rectangular Duct by a Laser-Induced Fluorescence Method

Handa, Taro
Department of Energy and Environmental Engineering, Interdisciplinary Graduate School of Engineering Sciences, Kyushu University

Masuda, Mitsuharu
Department of Energy and Environmental Engineering, Interdisciplinary Graduate School of Engineering Sciences, Kyushu University

Matsuo, Kazuyasu
Department of Mechanical Systems and Environmental Engineering, the University of Kitakyushu

https://doi.org/10.15017/16661

出版情報：九州大学大学院総合理工学報告. 24 (2), pp.179-185, 2002-09. 九州大学大学院総合理工学府
バージョン：
権利関係：

九州大学大学院総合理工学報告
第24巻 第2号 179-185頁 平成14年9月

Engineering Sciences Reports, Kyushu University
(KYUSHU DAIGAKU SOGORIKOGAKU HOKOKU)
Vol. 24, No. 2 pp. 179-185 SEPT. 2002

Three-Dimensional Structure of Normal Shock Wave/Turbulent Boundary Layer Interaction in a Rectangular Duct by a Laser-Induced Fluorescence Method

Taro HANDA*1,† Mitsuharu MASUDA*1 and Kazuyasu MATSUO*2
†E-mail of corresponding author: *handa@ence.kyushu-u.ac.jp*

(Received July 31, 2002)

The three-dimensional flow structure induced by normal shock wave/turbulent boundary-layer interaction in a constant area rectangular duct is investigated by a laser-induced fluorescence method. This diagnostic system uses an argon-ion laser with iodine seeded as fluorescence material. The Mach number distributions in the duct are obtained, and the structure of the flow field is clarified including the three-dimensional pattern of the boundary-layer separation induced by a shock wave.

Key words: *Laser-Induced Fluorescence, Shock Wave, Boundary Layer, Supersonic Flow*

1. Introduction

Normal shock wave/turbulent boundary-layer interaction (NSW/TBLI) generated in supersonic flows in a rectangular duct appears in various high-speed flow devices, for example, inlets of an airbreathing engine, supersonic ejectors, compressor cascades and supersonic nozzles. This interaction generates a highly three-dimensional flow structure due to four flat walls enclosing the duct, and influences the aerodynamic performance of the systems. Although its three-dimensional characteristics are of practical importance, not much work has been done on this problem.

Doeffer and Dallmann[1] investigated the three-dimensional characteristics of the flow with NSW/TBLI on a convex wall in a wind tunnel at a Mach number of 1.47. They controlled the boundary layer thickness and changed the Reynolds number based on the boundary layer thickness. With oil-flow visualization, they found that asymmetry of the oil-flow pattern increased substantially with Reynolds number, and a streamwise helical flow existed downstream of a shock wave.

Bejm et al.[2] made another experimental investigation with the same facility as Doeffer and Dallmann. They used two curved passages which had the same shape with a different span. Their results suggested that the three-dimensional flow characteristics depended strongly on the span.

Gerolymos et al.[3] described the three-dimensional character of the flow produced by the NSW/TBLI at the corners of a nozzle with rectangular cross-section by solving the Navier-Stokes equations with k-ε two-equation turbulence model. In their numerical results, a three-dimensional recirculation zone appeared in the corners.

In spite of the researches described above, important problems remain unsolved. These are; firstly, what is the three-dimensional character of an internal flow with NSW/TBLI?; secondly, how is that flow generated?; finally, what shape does a shock wave at a duct corner take? In order to answer these questions, we studied the flow in a duct with constant cross-sectional area. This shape was selected because it could extract the fundamental interaction phenomenon excluding the effect of the change in flow area.

In the present work three-dimensional distributions of flow field parameters were measured by a laser-induced fluorescence (LIF) method. This diagnostic system uses an argon-ion laser with iodine seeded as fluorescence material. When the pressure of the flow is nearly atmospheric, the rate of the collisional quenching of iodine molecules excited by an argon-ion laser dominates that of the spontaneous emission. In this pressure range, the LIF signal intensity is found to depend only on temperature under the condition that

*1 Department of Energy and Environmental Engineering
*2 Department of Mechanical Systems and Environmental Engineering, the University of Kitakyushu

an argon-ion laser is operated by the broad-band mode with a wavelength of 514.5nm and that the laser intensity is much less than the saturation intensity.[4)-6)] This indicates that the temperature distribution can be obtained from the LIF signal if the temperature of one specified point in the flow field is known. For the flow used in the present work, Mach number seemed more useful to consider the flow characteristics than temperature, so that temperature was converted to Mach number by assuming the flow being adiabatic.

In the present experiment, the laser beam sheet was injected into the duct from the downstream direction. The laser beam sheet was scanned across the flow field, and the two-dimensional LIF image of each scan was recorded by a CCD camera. The image data were stored into the computer, and the three-dimensional distribution of Mach number was calculated. With this method, the complicated flow field in the duct was clarified including the three-dimensional pattern of the boundary-layer separation induced by a shock wave.

2. Theory of LIF

When iodine molecules are excited by an argon-ion laser lasing with a broad-band mode of 514.5nm wavelength and with the power much lower than the saturation intensity, the LIF intensity is given as[7)],

$$S_F=\eta\, h\nu \frac{\Omega}{4\pi} V_c \frac{A}{A+Q}\frac{B}{c} I f N_{I_2} \qquad (1)$$

where η is the light collection efficiency, h the Planck's constant, ν the LIF frequency, Ω the LIF collection solid angle, V_c the measurement volume, A the spontaneous emission coefficient, B the stimulated emission coefficient, Q the collisional quenching rate, c the speed of light, I the laser intensity and f and N_{I_2} are the population fraction and number density of iodine molecules, respectively. When the pressure in the flow is nearly atmospheric, the spontaneous emission coefficient is much smaller than the collisional quenching rate. Then, equation (1) is written for the constant laser power as,

$$S_F= C\frac{1}{Q} f(T)\, N_{I_2} \qquad (2)$$

where

$$C\equiv \eta\, h\nu \frac{\Omega}{4\pi} V_c A \frac{B}{c} I=\text{const.} \qquad (3)$$

Since the population fraction f depends only on temperature T, f is expressed as $f(T)$ in the above equation. The collisional quenching rate Q can be written as,

$$Q= C'\frac{p}{\sqrt{T}} \qquad (4)$$

where p is the pressure and C' is the constant. The number density of iodine molecules is,

$$N_{I2} = p_{I2} / kT \qquad (5)$$

where p_{I2} is the partial pressure of iodine and k the Boltzmann constant. Since the seeding rate of iodine does not vary in the flow field, the p_{I2} is proportional to the pressure. Consequently, the LIF intensity is,

$$S_F= C_0\frac{f(T)}{\sqrt{T}} \qquad (6)$$

where C_0 is an another constant.

Equation (6) indicates that the LIF intensity depends only on temperature. Therefore, if the temperature and the LIF intensity are known at one specified point in the flow field, the constant C_0 is evaluated and LIF intensity distribution gives the temperature distribution of the flow field. In the calculation of $f(T)$, the quantum numbers that are taken into account are 0, 1 and 2 for the vibrational and 13 and 15 for the rotational quantum states, respectively.

In the flow field of polyatomic gases with high expansion rate, the flow can not maintain an equilibrium state and the difference occurs among the translational, rotational and vibrational temperatures[8)]. In this situation, the temperature obtained by LIF method is questionable. However, in the present experiment, the expansion of the gas is constrained by the walls of a duct and the maximum Mach number is less than 1.7, so that the nonequilibrium effect can be neglected.

In the present paper, a Mach number distribution is obtained from the temperature measured by a LIF method. To calculate a Mach number from temperature, the stagnation temperature is taken as constant over the entire flow field, that is, the flow is assumed as adiabatic. This approximation is verified in transonic and supersonic internal flows[9), 10)]. Mach number M is then calculated by the following equation,

$$\frac{T_0}{T}=1+\frac{\gamma-1}{2} M^2, \qquad (7)$$

where T_0 is the stagnation temperature.

3. Diagnostic system

The LIF diagnostic system and experimental setup are shown in Fig. 1, where (1) ~ (5) correspond to the diagnostic system. The laser is an argon-ion laser (Spectra Physics, model 2017, 5W) with a prism in the cavity and is lased with a broad-band mode of 514.5nm wavelength. In the experiment, the laser power is adjusted to 1W. Considering the thickness of the laser beam in the duct, this power is about 1/1000 of the saturation intensity of fluorescence. The laser beam is shaped to a sheet with a thickness of 0.5mm through one convex lens (15mm focal length) and two cylindrical lenses (100mm and 1000mm focal lengths), and it is injected into the duct from the downstream direction. The resulting LIF signal is measured from the direction perpendicular to the laser beam sheet. The signal is collected by lenses (Nikon, F 1.4) and detected by the CCD camera with image intensifier. The laser collimation and collection optics are moved to scan in the depth direction of the duct, and the LIF images for each scan is stored in the computer. With this procedure, the three-dimensional distribution of the LIF intensity is obtained, and the temperature distribution on specified plane is analyzed.

The sensitivity of an image intensifier is not uniform over the plane of its output phosphor. Also, due to the upper and lower walls of the duct, solid angle of the LIF collection optics is not the same for images taken at different locations. To take these effects into account, the diagnostic system is calibrated by filling the still air with iodine seed in the duct. This still air is irradiated by the laser and, by scanning the optical system, the LIF signals are recorded for each plane where the LIF image of the flow field is to be taken. By using these as reference images, the image data of the flow field are corrected.

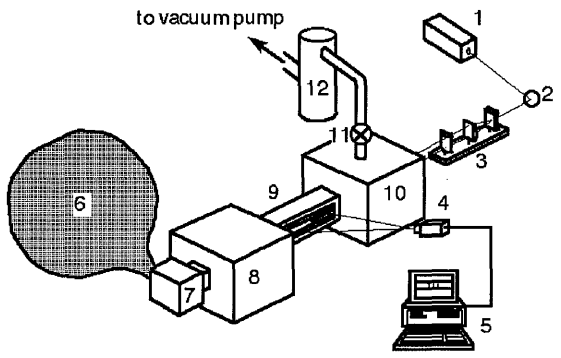

1. A laser　2. mirror　3. cylindrical lens
4. ICCD camera　5. personal computer
6. balloon　7. iodine cell　8. stagnation chamber
9. duct　10. expansion chamber
11. valve　12. vacuum tank

Fig. 1 Measuring system and experimental setup

The spatial resolution of the present diagnostic system is determined by the thickness of the laser beam sheet in the depth direction and is less than 0.5mm. On the image plane, the simple geometrical consideration shows that one pixel of the image plane corresponds to the physical size of 0.09mm × 0.09mm. To estimate the resolution accurately, however, it is necessary to clarify the integrated resolution including the characteristics of collection optics, the image intensifier, the CCD camera and the frame-digitizer in the computer. Therefore, we made a experiment similar to McMillin et al.[9] and took the image of a knife-edge. According to this experiment, the image of the knife-edge is found to be recorded in 4 pixels, so that the one pixel corresponds to the 0.36mm × 0.36mm. The temporal resolution is limited by the framing rate of the CCD camera and is 1/30s.

4. Experimental setup and method

The experimental setup is shown by (6) ~ (12) in Fig. 1. The wind tunnel is a blow-down type operated by dry nitrogen with atmospheric pressure and temperature. The dry nitrogen has water content less than 5ppm, and the condensation in the duct is avoided by using this gas. The vacuum tank (12) in Fig. 1 is evacuated to a pressure less than 13kPa by closing the valve (11), then the dry nitrogen contained in the balloon (6) is introduced into the iodine cell, where iodine is sublimated into nitrogen. The nitrogen with a small amount of iodine (~4wt%) is supplied to the test duct (9) through the stagnation chamber (8). The duration of the wind tunnel is limited by the pressure increase in the vacuum tank and is about 60s. The pressure and temperature in the stagnation chamber are maintained at 1.012×10^5Pa and 293.3K, respectively.

Figure 2 shows the detailed structure of the test duct. The Mach number at the entrance of a constant area cross-section is 1.68. This value is calculated from the time-averaged static pressure on the side wall, the stagnation pressure and temperature in the

plenum chamber. The coordinate used to analyze results is shown in Fig.3, where x, y, and z are the streamwise, transverse and depth coordinates, respectively.

The flow field is scanned in the depth direction from z=0.5mm to z=19.5 mm with a step of 1 mm by the laser beam sheet formed in the x-y plane. It takes at least 1/30s to obtain the LIF image data for one scan. In the present experiment, the pressure is nearly atmospheric. This means that the collisional quenching of the excited iodine molecule is large, resulting in the low LIF intensity. Therefore, the one LIF image taken in 1/30s is degraded by the noise due to the photon statistics. To avoid this problem, ten images are taken successively for each one physical plane and are averaged. The very clear images are obtained

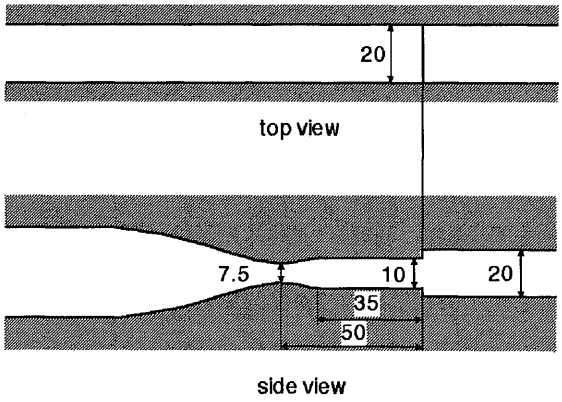

Fig. 2 Test model

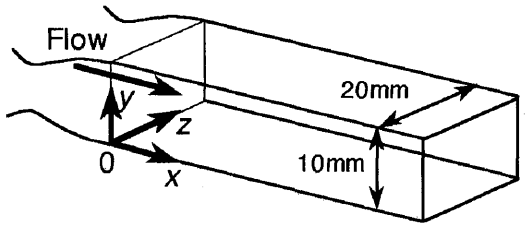

Fig. 3 Coordinate system

by this procedure.

As described earlier, the temperature of the one specified point should be known to obtain its distributions over the whole flow field. In the present experiment, this point is taken at x=3mm, y=5mm, and z=9.5mm, and the reference temperature is calculated from the time-averaged static pressure on the side wall, the stagnation pressure and temperature in the plenum chamber.

Inoue et al. checked the accuracy of the temperature measurement with the same diagnostic system by using the flow in a two-dimensional transonic nozzle[4), 5)]. The temperatures obtained by the LIF method were compared with those calculated from the measured values of the stagnation and static pressures on the nozzle side-wall by assuming the flow being adiabatic. Both values agree within $\pm$3K. The range of flow parameters in the present experiment is almost identical with this calibration experiment, so that the similar accuracy is obtained in the present duct flow.

5. Results and discussion

Figure 4 shows a Mach number contour on the x-z plane at y=5mm. There is a subsonic region downstream of x~10mm. The initial normal shock wave stands at this location, and a flow is decelerated through it from supersonic to subsonic speed. The minimum Mach number in this region is 0.93. The deceleration through the normal shock wave is gradual because the flow is unsteady and the shock wave oscillates in the streamwise direction.

In Fig. 4, a flow near a wall is seen supersonic both upstream and downstream of the initial shock wave. The shock wave is bifurcated near the wall and the flow is decelerated through two oblique shock waves. According to Kooi[11)], the strength of the trailing leg of this bifurcation is determined from the condition that the static pressure across the slip surface must be equal. This condition dictates that the flow is subsonic in the downstream of the trailing leg. It is noted from Fig. 4, however, that the experimental data suggest this region being supersonic. This contradiction is probably caused by the fact that the shock wave is not stationary but oscillating around its time-averaged position.

When the flow Mach number is greater than 1.3[12), 13)], the normal shock wave in the flow generally separates the boundary layer due to its strong adverse pressure gradient. This separation increases the boundary layer thickness and, consequently, decreases the effective cross-sectional area of the duct. The subsonic flow behind a shock wave is then accelerated to supersonic speed. In addition to this effect, a flow that has passed bifurcation has higher Mach number than that through a normal shock wave. This effect is seen in Fig. 4 as a region enclosed with the contour line of M=1.2. The supersonic flow downstream of the first shock wave is decelerated again by the second normal

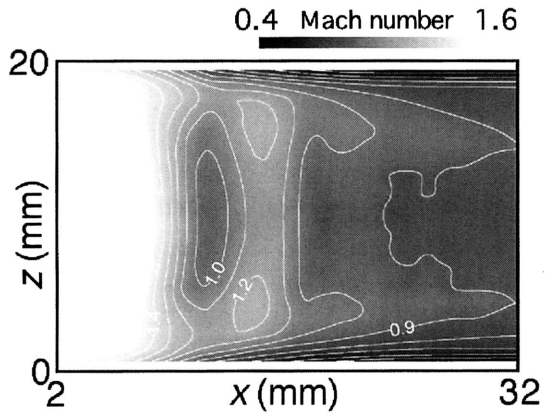

Fig. 4 Mach number contour on x-z plane at y=5mm

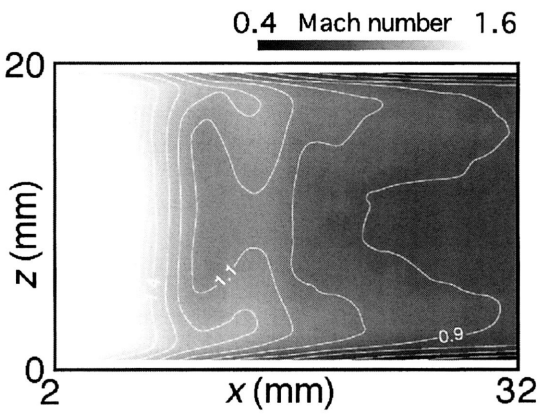

Fig. 6 Mach number contour on x-z plane at y=2mm

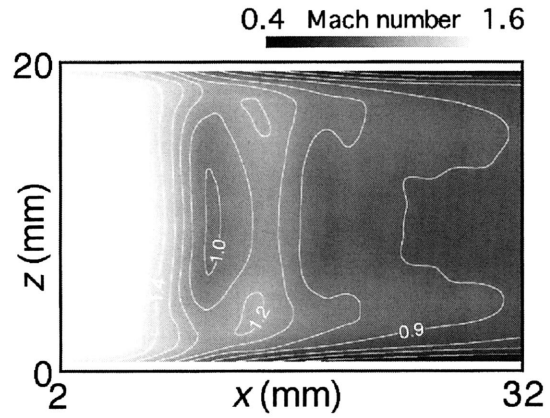

Fig. 5 Mach number contour on x-z plane at y=3mm

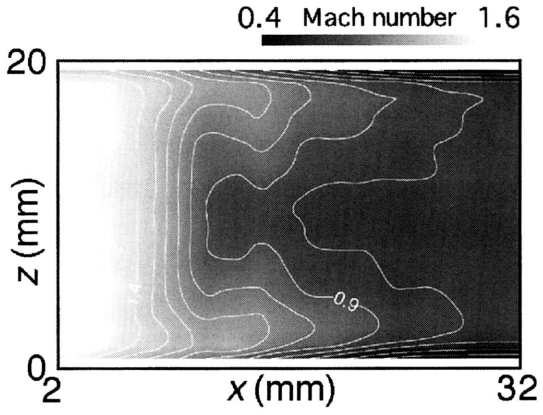

Fig. 7 Mach number contour on x-z plane at y=1mm

shock wave.

This flow pattern has already been described by Carroll et al. They obtained the two-dimensional Mach number contour of a flow for the inlet Mach number of 1.6 by the LDV method[9], and computed this flow by solving the Navier-Stokes equations with k-ω^2 turbulence model[14]. The characteristic features of their results are very well reproduced in Fig. 4.

The Mach number contours shown in Figs. 4 ~ 7 indicate that the subsonic region behind the initial shock wave on the plane at y=3mm is smaller than that at y=5mm, and this region disappears on the plane at y=2mm. This indicates that the subsonic region behind the shock wave is located near the central portion of the duct cross-section and is surrounded by the supersonic region. On the other hand, two regions having locally higher Mach numbers (enclosed by the contour line of 1.2) become small with the decrease of y for $y \geq 3$mm, and then merge into the upstream region with higher Mach number at y=2mm. Finally the shape of Mach number contour lines looks like two horns at y=1mm. Since the change in an effective cross-section along the flow is highly three-dimensional, the acceleration and deceleration of the flow are very complicated as shown in Figs. 4 ~ 7.

Figure 8 shows Mach number contour on the y-z plane at x=12mm, just behind the shock wave. At four corners of the duct, the high Mach number regions enclosed by the contour line of 1.2 are seen to exist and the boundary layers are thin compared with those on the walls near the duct center. This behavior of wall boundary layers is also evident in the downstream region as shown in Figs. 9 and 10.

In order to explain the flow field described above, shock waves are assumed to take configurations depicted in Fig. 11. On a plane away from the side wall (plane A), a shock wave takes a λ–shape. On the other hand, at the corner of a duct, the bifurcated shock wave developed on a lower wall interacts with that on a side wall, and the configuration on a plane near the side wall (plane B) becomes very complicated. On the plane A, a flow near the lower wall passes

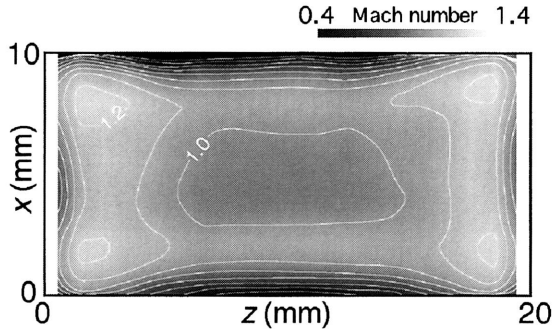

Fig. 8 Mach number contour on y-z plane at x=12mm

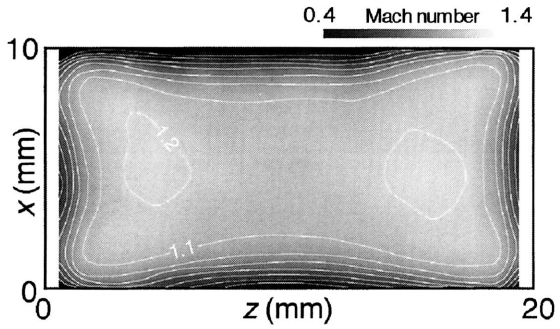

Fig. 9 Mach number contour on y-z plane at x=16mm

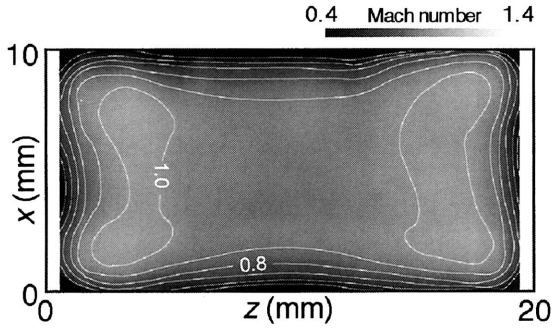

Fig. 10 Mach number contour on y-z plane at x=20mm

two oblique shock waves generated by bifurcation. On the other hand, a flow in a corner region passes three oblique shock waves as shown in the figure of the plane B. The Mach number behind the terminal oblique shock wave is determined by the condition that the static pressure at this location must be uniform over the entire cross-section of the duct. This consideration indicates that the adverse pressure gradient across the two oblique shock waves on the plane A becomes large compared with that across the three oblique shock waves on the plane B. As a result, the boundary layer at the stem of a terminal oblique shock wave on the plane A becomes thicker than that on the plane B. The flow pattern thus assumed can explain the boundary layer shape shown in Figs. 8, 9, and 10.

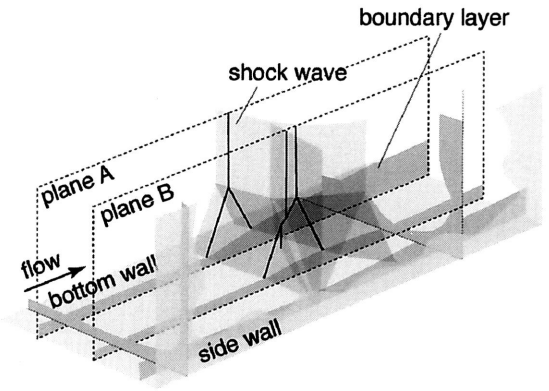

Fig. 11 Structure of the shock wave at a duct corner

Figure 8 also indicates that the Mach number near a duct corner is high compared to the other part of the flow. It is probably caused by that the flow in this region is decelerated by many weak oblique shock waves.

6. Concluding remarks

Three-dimensional flow structure of normal shock wave/turbulent boundary layer interaction (NSW/TBLI) in a constant area rectangular duct was investigated by a laser-induced fluorescence method. This system used an argon-ion laser as a light source, and the target gas was dry nitrogen seeded with iodine. By operating the laser with a broad-band mode, the temperature distribution in the flow was obtained, and it was converted to the Mach number distribution by assuming the flow being adiabatic.

The results revealed that the flow induced by NSW/TBLI was highly three-dimensional and complicated. A local high Mach number region was found to exist in duct corners immediate downstream of the initial shock wave. A boundary layer near a corner was very thin compared with that on the wall of a central part of the duct. These flow characteristics were thought to be caused by the interaction between two bifurcated shock waves developed on the two perpendicularly adjacent walls. The simple flow model was constructed and it was shown that this model could explain very well the experimental results.

References

1) Doerffer, P. and Dallmann, U., "Reynolds Number Effect on Separation Structures at Normal Shock Wave/Turbulent Boundary-Layer Interaction," *AIAA J.*, Vol. 27, No. 9, 1989, pp.1206-1212.

2) Bejm, M., Doerffer, P. and Kania, W., "An Effect of Test Section Span on the Shock Wave - Turbulent Boundary Layer Interaction," 4th Int. Symp. on Experimental and Computational Aerothermodynamics of Internal Flows, Vol. I, 1999, pp.102-110.

3) Gerolymos, G.A., Vallet, I., Bölcs, A. and Ott, P., "Computation of Unsteady Three-Dimensional Transonic Nozzle Flows Using k-ε Turbulence Closure," *AIAA J.*, Vol. 34, No. 7, 1996, pp.1331-1340.

4) Inoue, M., Muraishi, T., Masuda, M. and Natsunari, K., "Visualization of Transonic Flow in Curved Nozzle with Rectangular Cross-Section by Laser-Induced Fluorescence Method," J. Flow Visualization Society of Japan, Vol. 10, 1990, pp.103-106 (in Japanese).

5) Inoue, M., Masuda, M. and Muraishi, T., "Visualization of Transonic Nozzle Flow by Laser-Induced Fluorescence Method," J. Flow Visualization Society of Japan, Vol. 11, 1991, pp.35-42 (in Japanese).

6) Hartfield, R.J., Hollo, S.D. and McDaniel, J.C., "Planar Temperature Measurement in Compressible Flows Using Laser-Induced Fluorescence," Optics Letters, Vol. 16, No.2, 1991, pp.106-108.

7) McDaniel, Jr.J.C., "Investigation of Laser-Induced Iodine Fluorescence for the Measurement of Density in Compressible Flows," Stanford Univ., SUDAAR, No.532, 1982.

8) Soga, T. and Niwa, K., "On the Rotational and Transitional Nonequilibrium in an Under-expanded Free Jet of Nitrogen," Trans. of the Japan Society for Aeronautical and Space Sciences, Vol. 28, 1985, pp.16-26.

9) Carroll, B.F. and Dutton, J.C., "Multiple Normal Shock Wave/Turbulent Boundary-Layer Interactions," J. Propulsion and Power, Vol. 8, No.2, 1992, pp.441-448.

10) Cahen, J., Couaillier, V., Délery, J. and Pot, T., "Validation of Code Using Turbulence Model Applied to Three-Dimensional Transonic Channel," *AIAA J.*, Vol. 33, No. 4, 1995, pp.671-679.

11) Kooi, J.W., "Experiment on Transonic Shock-Wave Boundary Layer Interactions," AGARD No. 168, 1975.

12) Bogar, T.J., Sajben, M. and Kroutil, J.C., "Characteristics Frequencies of Transonic Diffuser Flow Oscillations," *AIAA J.*, Vol. 21, No. 9, 1983, pp.1232-1240.

13) Sajben, M. and Kroutil, J.C., "Effects of Initial Boundary-Layer Thickness on Transonic Diffuser Flows," *AIAA J.*, Vol. 19, No. 11, 1981, pp.1386-1393.

14) Carroll, B.F., Lopez-Fernandez, P.A. and Dutton, J.C., "Computations and Experiments for a Multiple Normal Shock/Boundary-Layer Interaction," J. Propulsion and Power, Vol. 9, No. 3, 1993, pp.405-411.